Boundary Effects in Confined Copolymer System and Compressible SCFT Model

Weiquan Xu and Pingwen Zhang*

School of Mathematical Sciences,

Peking University,

Beijing 100871, China

(Dated: December 1, 2009)

The conventionally used Modified Self-consistent Field Theory (MSCFT) for confined system is known to have two major difficulties: numerical instability and too many artificial constrains. Here we propose a modified Compressible Model based Selft-consistent Field Theory (CMSCFT), which has no artificial constrains and gives satisfactory simulations of all known hard-surface effects including surface depletion, surface density oscillation, and surface segregation. We also show that CMSCFT converges to conventional Self-consistent Field Theory (SCFT) when compressibility tends to zero. Therefore, we suggest that CMSCFT will be a promising tool when dealing with copolymer systems with hard surface confinements.

Keywords: Compressible Model; Boundary Layer; Boundary Effect.

INTRODUCTION

Self-assembly behavior of block polymers is an effective and efficient method to create structures at nanometer scale which encourages various potential applications including lithographic templates for nano-wires, photonics crystals, and high-density magnetic storage media [1]. As a consequence, block polymers have been the focus of academic community in the past decades. Until recently, plenty of great improvements have been achieved and SCFT is proved to be one of the most powerful tools that successfully characterizes block copolymer melt system without confinements [2–5].

However, things become much more complicated when we consider confinement effects which can influence self-assembly behaviors in the bulk [6, 7]. Asakura and Oosawa [8] suggested long ago that the loss of configurational entropy of polymers in the proximity to the hard wall should lead to a strong steric repulsion called "entropy repulsion", giving rise to the depletion of density profile near surface. The competition between the packing constraints and the loss of configurational entropy in the vicinity of the hard wall leads to more complicated polymer interfacial behavior, e.g. surface depletion [9, 10], surface density oscillation [11, 13], and surface segregation [14]. Thus, the behavior of polymer melts at hard surfaces requires much more efforts than simple liquids.

Confinement effects of copolymer melt are also associated with many scientific challenges and technological applications [15], and have drawn increasing interest in the community.

The interest in this field can date back to 1979, when Joany *et al.* first obtained the density profile of polymer solutions [16] by mean-field theory. This result was later confirmed by Allain's direct optical observation, and the profile is shown to be expressed as the square of a hyperbolic tangent [9]:

$$\rho(x) = \tanh^2\left(\frac{x}{\delta}\right), \tag{1}$$

where δ is the depletion layer thickness. It is striking to note that, Eq. (1) is exactly the same as the profile established by Van der Waals for the interface between the co-existing fluid phases of a binary mixture in 1894 [17]. Later on, J. N. Israelachvili and coworkers performed measurements of equilibrium surfaces force of various systems: poly-dimethylsiloxane (PDMS) with up to 50 monomer units per molecule [18], and two samples of liquid polybutadienes (PB) with about $n \approx 20$ and $n \approx 65$ segments [13]. In the case of PDMS, experiment shows large oscillations of the surface force when the distance (called D) between two mica surface is below $\sim 5\,nm$. However, the two PB samples show simply steeply repulsive force: effectively an impenetrable "hard wall" at $D \approx 3.0nm$ and $D \approx 3.7nm$, respectively. These results reveal much important information about surface force of confined copolymer melt systems, though the force law in the area closer to $D = 0$, e.g. $D \in (0, 3nm)$, has not been established yet. Furthermore, a review of recent experimental work about polymer-induced forces near hard surfaces was given by Kleshchanok *et al.* [19], where limited theoretical work about surface potential was also mentioned. In Kleshchanok's review, the Derjaguin approximation [20, 21] is highly regarded as a powerful tool computing potential near more complicated surfaces, e.g. sphere and cylinder.

Simultaneously, plenty of computational simulations were also devoted to confinement effects. Monte Carlo simulations were first studied by Kikuchi and Binder [22]. Later, Matsen developed a Modified Self-consistent Field Theory (MSCFT) for confined copolymer systems [23]. In the framework of conventional SCFT, incompressibility constraint requires the total polymer segmental density to be uniform (normalized as 1 in volume fraction). However, hard wall constraint requires the polymer density to vanish at the surface. In Ref [23], Matsen generalized this incompressibility condition, and enforced the total segment density to an arbitrarily predesigned profile ϕ_0 which continuously increases from 0 to 1 in the vicinity of the boundary. This method was widely used in the subsequent research: just like Matsen, Geisinger *et al.* used cosine-shape profile to examine the phase stability

[24]; Chen and Fredrickson adopted a linear profile in ABC triblock thin film [25]; Li *et al.* chose a "step-function" profile under cylinder confinement [26]. Unfortunately, this widely used method have some inherent problems, such as numerical instability as well as the incorporation of arbitrary profiles. Although Q. Wang *et al.* recently tried to amend the method by selecting a "best" profile that reduces numerical instability, it is hard to say that they have got a truly physical profile [27]. In addition, in Q. Wang's paper, boundary layer thickness is so artificial that no rule is known to fix it. Finally, it is improper to guess "suitable" profile for various block copolymer melt systems. In light of these difficulties, we propose this CMSCFT, in the hope that it can be a useful improvement to the current theory.

In the present paper, we introduce Helfand's harmonic penalty function [28] in compressible SCFT framework, and use it to examine all boundary effects thoroughly. We should mention that, this idea is inspired from the compressible model of homopolyer solution in Fredrickson's monograph [29]. All parameters in CMSCFT have clear physical backgrounds. Boundary potentials are constructed through physical analysis and experimental inspiration from Israelachvili *et al.* [13, 18, 19]. Compressibility $1/\zeta$ can also be fixed by comparing numerical simulations and experimental measurements. The boundary layer profile from our simulations has a good agreement with experimental results [9] and emprical formula (1). Finally, our simulation describes all known hard surface effects: surface density depletion, oscillation, and surface segregation. The rest of this article is organized as follows: in Sec. II, we introduce Compressible Model and numerical method; Sec. III shows the CMSCFT simulations of boundary effects, and comparison with similar or relative works is also given; concluding remarks are given in Sec. IV.

COMPRESSIBLE MODEL

Suppose the AB diblock copolymer melt system, called $\boldsymbol{R}$, has n copolymers which described as Gaussian chains $r_j(s)$ with $j = 1, 2, \cdots n$. We use N to represent the total number of segments per copolymer, and f for copolymer composition: $s \in [0, f]$ for A segments and the rest for B segments. And $\rho_0 = \frac{nN}{V}$ is the total segment density, where V is the system

volume. So normalized segment density operators can be written as:

$$\begin{aligned}\hat{\rho}_A(\boldsymbol{r}) &= \frac{N}{\rho_0}\sum_{j=1}^{n}\int_0^f ds\delta(\boldsymbol{r}-\boldsymbol{r}_j(s)),\\ \hat{\rho}_B(\boldsymbol{r}) &= \frac{N}{\rho_0}\sum_{j=1}^{n}\int_f^1 ds\delta(\boldsymbol{r}-\boldsymbol{r}_j(s)),\end{aligned} \tag{2}$$

where $\hat{\rho}_A(\boldsymbol{r})$ and $\hat{\rho}_B(\boldsymbol{r})$ are segment density for A and B, respectively. The Hamiltonian in this system includes both elastic potential energy of Gaussian chain $U_0[\boldsymbol{R}]$ and short-range interaction between AB segments $U_1[\boldsymbol{R}]$, as given below:

$$\begin{aligned}\beta U_0[\boldsymbol{R}] &= \frac{3}{2Nb^2}\sum_{j=1}^{n}\int_0^1 ds\left|\frac{d\boldsymbol{r}_j(s)}{ds}\right|^2\\ \beta U_1[\boldsymbol{R}] &= \frac{\varepsilon_{AA}\rho_0}{2}\int d\boldsymbol{r}\hat{\rho}_A\hat{\rho}_A + \frac{\varepsilon_{BB}\rho_0}{2}\int d\boldsymbol{r}\hat{\rho}_B\hat{\rho}_B + \varepsilon_{AB}\rho_0\int d\boldsymbol{r}\hat{\rho}_A\hat{\rho}_B,\end{aligned} \tag{3}$$

where we assume that A and B particles have the same statistical segment length b and ε_{IJ} is the cohesive interaction between segments of type I and J. Incompressibility in conventional SCFT framework requires uniform density: $\hat{\rho}_A(\boldsymbol{r})+\hat{\rho}_B(\boldsymbol{r}) = 1$ throughout the system, which is ensured by a δ-functional in the partition function.

$$Z = \int\prod_{j=1}^{n}\mathcal{D}\boldsymbol{r}_j\cdot\delta[\hat{\rho}_A+\hat{\rho}_B-1]\cdot\exp\left\{-\frac{H\{\boldsymbol{R}\}}{k_BT}\right\} \tag{4}$$

In order to satisfy the hard wall constraint, Matsen constrained the total density to be a predesigned profile ϕ_0 by a modified δ-functional [23]:

$$Z = \int\prod_{j=1}^{n}\mathcal{D}\boldsymbol{r}_j\cdot\delta[\hat{\rho}_A+\hat{\rho}_B-\phi_0]\cdot\exp\left\{-\frac{H\{\boldsymbol{R}\}}{k_BT}\right\} \tag{5}$$

In CMSCFT, we use Helfand's harmonic penalty function [28] instead to characterize incompressibility:

$$\beta U_2[\boldsymbol{R}] = \frac{1}{2}\zeta\rho_0\int d\boldsymbol{r}\left(\hat{\rho}_A+\hat{\rho}_B-1\right)^2 \tag{6}$$

Note that $1/\zeta$ is the measurement of compressibility: the system becomes incompressible when $\zeta\to\infty$. Generally, the energy of polymer-boundary interaction is written as integration of given boundary potential $J(\boldsymbol{r})$:

$$\beta U_3[\boldsymbol{R}] = \rho_0\int d\boldsymbol{r}\left(\hat{\rho}_A+\hat{\rho}_B\right)\cdot J(\boldsymbol{r}) \tag{7}$$

Now the system Hamiltonian has two more terms than the conventional case:

$$H\{\boldsymbol{R}\} = U_0[\boldsymbol{R}] + U_1[\boldsymbol{R}] + U_2[\boldsymbol{R}] + U_3[\boldsymbol{R}]. \tag{8}$$

And the partition function of compressible model can be written as functional integration without δ-functional:

$$Z = \int \prod_{j=1}^{n} \mathcal{D}\boldsymbol{r}_j \cdot \exp\left\{-\frac{H\{\boldsymbol{R}\}}{k_B T}\right\} \tag{9}$$

We should mention that a superfluous assumption was made due to technical difficulty in deriving field-based formulation: segment-segment interaction is assume to be equal ($\varepsilon_{AA} = \varepsilon_{BB} = \varepsilon$). With this assumption, the field-based Hamiltonian of compressible model can be obtained through a Hubbard-Stratonovich transformation. Interested readers are referred to, e.g., Ref. [5, 29] for detailed derivation. Consequently, field-theoretic Hamiltonian of compressible model can be fixed as follows up to an unimportant constant which makes no difference of the SCFT model:

$$\begin{aligned}\frac{H[\mu_+,\mu_-]}{n} = \frac{1}{V}\left[\frac{1}{\chi N}\int d\boldsymbol{r}\mu_-^2 - \int d\boldsymbol{r}\mu_+\right] - \ln Q\left[\mu_+,\mu_-\right] \\ + \frac{1}{V[\chi N + 2(\zeta+\varepsilon)N]}\int d\boldsymbol{r}\Big\{\left[2J(\boldsymbol{r}) + \bar{\varepsilon}\right]\cdot N\cdot\mu_+ - \mu_+^2\Big\},\end{aligned} \tag{10}$$

where $\bar{\varepsilon} = \varepsilon_{AB} + \varepsilon$, $\chi = \varepsilon_{AB} - (\varepsilon_{AA} + \varepsilon_{BB})/2 = \varepsilon_{AB} - \varepsilon$ is Flory segment-segment interaction parameter, $Q[\mu_+,\mu_-]$ is single-chain partition function, μ_+ is the fluctuation pressure field and μ_- is exchange chemical potential field. It is convenient to introduce equivalent fields w_A and w_B on the A, B segments, where

$$\begin{aligned} w_A &= \mu_+ - \mu_- \\ w_B &= \mu_+ + \mu_- \end{aligned} \tag{11}$$

At the same time, field based partition function can be written as:

$$Z = \int \mathcal{D}\mu_+\mathcal{D}\mu_- \cdot \exp\left\{-\frac{H[\mu_+,\mu_-]}{k_B T}\right\} \tag{12}$$

Saddle point approximation, which takes maximum along μ_+ direction and minimum along μ_- direction, is used to calculate the Partition Function (12). And hence free energy in the vicinity of equilibrium state approximates the field based Hamiltonian (10). Consequently, finding equilibrium state is equivalent to finding the saddle point of Hamiltonian

(10). $F[\mu_+,\mu_-]=H[\mu_+,\mu_-]/n$ is introduced as free energy for convenience. We can use the well-known steepest update strategy to approximate the saddle point:

$$\begin{aligned}\frac{\delta F[\mu_+,\mu_-]}{\delta\mu_+}&=\frac{2}{V[\chi N+2(\zeta+\varepsilon)N]}\left\{\left[J(\boldsymbol{r})+\frac{\bar{\varepsilon}}{2}\right]\cdot N-\mu_+\right\}+\frac{1}{V}\left[\rho_A+\rho_B-1\right]\\ \frac{\delta F[\mu_+,\mu_-]}{\delta\mu_-}&=\frac{1}{V}\left[\frac{2}{\chi N}\mu_-+\rho_B-\rho_A\right],\end{aligned}\tag{13}$$

where ρ_A,ρ_B are real density of A, B segments respectively. They can be computed by way of backward and forward propagators $q^+(\boldsymbol{r},s)$, and $q(\boldsymbol{r},s)$:

$$\begin{aligned}\rho_A&=\frac{V}{Q}\int_0^f dsq(\boldsymbol{r},s)q^+(\boldsymbol{r},1-s)\\ \rho_B&=\frac{V}{Q}\int_f^1 dsq(\boldsymbol{r},s)q^+(\boldsymbol{r},1-s)\\ Q&=\int d\boldsymbol{r}q(\boldsymbol{r},s)q^+(\boldsymbol{r},1-s)\\ &=\int d\boldsymbol{r}q(\boldsymbol{r},1)=\int d\boldsymbol{r}q^+(\boldsymbol{r},1)\end{aligned}\tag{14}$$

Propagators are statistical weight of segments located sN units along the chain contour at point $\boldsymbol{r}$ with initial condition $q^+(\boldsymbol{r},0)=1,q(\boldsymbol{r},0)=1$:

$$\begin{aligned}\frac{\partial q(\boldsymbol{r},s)}{\partial s}&=\Delta_r q(\boldsymbol{r},s)-w_A(\boldsymbol{r})q(\boldsymbol{r},s), &s\leqslant f\\ \frac{\partial q(\boldsymbol{r},s)}{\partial s}&=\Delta_r q(\boldsymbol{r},s)-w_B(\boldsymbol{r})q(\boldsymbol{r},s), &s>f\\ \frac{\partial q^+(\boldsymbol{r},s)}{\partial s}&=\Delta_r q^+(\boldsymbol{r},s)-w_B(\boldsymbol{r})q^+(\boldsymbol{r},s), &s\leqslant f\\ \frac{\partial q^+(\boldsymbol{r},s)}{\partial s}&=\Delta_r q^+(\boldsymbol{r},s)-w_A(\boldsymbol{r})q^+(\boldsymbol{r},s), &s>f\end{aligned}\tag{15}$$

Our goal is to vanish the right hand side of equation (13). From measurements by Israelachvili *et al.* [13, 18, 19], we know that boundary potentials grow rapidly to ∞ when $\boldsymbol{r}$ is approaching the boundary, which can cause some computational difficulties: 1) it is hard to vanish the right hand side of the first equation in (13) because of numerical error, 2) extreme singularity of equivalent field w_A,w_B near surfaces brings stability problem of PDE (15). To avoid excessive numerical error, we recommend a temporary field when updating the gradient of Hamiltonian in formula (13):

$$\tilde{\mu}_+=\mu_+-\left[J(\boldsymbol{r})+\frac{\bar{\varepsilon}}{2}\right]\cdot N$$

At the same time implicit treatment of the entire right hand side is adopted in numerical approach to ensure unconditional stability when solving propagators (15).

It is important to note that, if we consider a free system without boundary influence ($J(\boldsymbol{r}) = 0$), the compressible model above converges to conventional incompressible model in the limit $\zeta \to \infty$:

$$\frac{H[\mu_+, \mu_-]}{n} \to \frac{1}{V}\left[\frac{1}{\chi N}\int d\boldsymbol{r}\mu_-^2 - \int d\boldsymbol{r}\mu_+\right] - \ln Q\left[\mu_+, \mu_-\right],$$

where the right hand side of the above formula is exactly field-theoretic Hamiltonian of conventional SCFT (regardless of a constant shift).

More generally speaking, boundary potential $J(\boldsymbol{r})$ on segment A,B should be different. Thus the energy of polymer-boundary interaction is written as:

$$\begin{aligned}\beta U_3[\boldsymbol{R}] &= \rho_0 \int d\boldsymbol{r}\Big[\hat{\rho}_A \cdot J_A(\boldsymbol{r}) + \hat{\rho}_B \cdot J_B(\boldsymbol{r})\Big] \\ &= \rho_0 \int d\boldsymbol{r}\Big[(\hat{\rho}_A + \hat{\rho}_B) \cdot J_+(\boldsymbol{r}) + (\hat{\rho}_A - \hat{\rho}_B) \cdot J_-(\boldsymbol{r})\Big],\end{aligned} \tag{16}$$

where $J_+(\boldsymbol{r})$ and $J_-(\boldsymbol{r})$ are just notations for convenience:

$$\begin{aligned}J_+(\boldsymbol{r}) &= \frac{J_A(\boldsymbol{r}) + J_B(\boldsymbol{r})}{2} \\ J_-(\boldsymbol{r}) &= \frac{J_A(\boldsymbol{r}) - J_B(\boldsymbol{r})}{2}\end{aligned}$$

By using a same procedure as above, we can determine the Hamiltonian for compressible model up to an unimportant constant:

$$\begin{aligned}\frac{H[\mu_+, \mu_-]}{n} = &\frac{1}{V}\left\{\frac{1}{\chi N}\int d\boldsymbol{r}\Big[\mu_-^2 + 2N \cdot J_-(\boldsymbol{r}) \cdot \mu_-\Big] - \int d\boldsymbol{r}\mu_+\right\} - \ln Q\left[\mu_+, \mu_-\right] \\ &+ \frac{1}{V[\chi N + 2(\zeta + \varepsilon)N]}\int d\boldsymbol{r}\Big\{\left[2J_+(\boldsymbol{r}) + \bar{\varepsilon}\right] \cdot N \cdot \mu_+ - \mu_+^2\Big\},\end{aligned} \tag{17}$$

where $\bar{\varepsilon} = \varepsilon_{AB} + \varepsilon$. Then variational gradient (13) for steepest update strategy is written as:

$$\begin{aligned}\frac{\delta F[\mu_+, \mu_-]}{\delta \mu_+} &= \frac{2}{V[\chi N + 2(\zeta + \varepsilon)N]}\left\{\left[J_+(\boldsymbol{r}) + \frac{\bar{\varepsilon}}{2}\right] \cdot N - \mu_+\right\} + \frac{1}{V}\left[\rho_A + \rho_B - 1\right], \\ \frac{\delta F[\mu_+, \mu_-]}{\delta \mu_-} &= \frac{1}{V}\left\{\frac{2}{\chi N}\Big[\mu_- + N \cdot J_-(\boldsymbol{r})\Big] + \rho_B - \rho_A\right\}.\end{aligned} \tag{18}$$

In order to reduce excessive numerical error, we need another intermediate field:

$$\tilde{\mu}_- = \mu_- + N \cdot J_-(\boldsymbol{r}).$$

In numerical simulations, we recommend the following four-order formula to discretize the modified diffusion equation (15):

$$\frac{25}{12}q^{n+1} - \delta s \cdot \Delta q^{n+1} + \delta s \cdot w \cdot q^{n+1} = 4q^n - 3q^{n-1} + \frac{4}{3}q^{n-2} - \frac{1}{4}q^{n-3} \tag{19}$$

The initial value of first four steps of (19) can be fixed by stable lower order method (like backward Euler discretization) and extrapolation. Because of the singularity of field $w_{A(B)}$ and resulting strong fluctuation of density profile near the boundary, non-uniform grids are also recommended. In fact, finite element implementation was used in this paper for convenience.

RESULTS AND DISCUSSION

For simplicity, our simulation only considers lamellae phase of diblock copolymer melt thin films, which can be reduced to a 1-D case. We note that, all simulations can be directly applied to 3-D case without difficulty but would require much more computational effort. The parameters are fixed as follows in the simulation, unless mentioned otherwise:

$$\varepsilon_{AA} = \varepsilon_{BB} = 0.1, \quad \varepsilon_{AB} = 0.2; \quad N = 120, \quad f = 0.48, \quad L = 4\pi \cdot R_g,$$

where, L is the thickness of thin films and R_g is polymer's unperturbed radius of gyration. Note that SCFT involves multi-solutions. All those equilibrium states we get from simulations should be meta-stable phase that relies significantly on initial fields we assign before hand. In the following simulations, we set $\mu_+ = 0,\ \mu_- = 1$ which has no inclination to any special density profile pattern.

Model Comprison

In systems without hard surface confinement, where periodic boundary condition was used to compute propagators (15), CMSCFT gradually converges to conventional SCFT when compressibility $1/\zeta$ drops to zero. Of course, boundary potential in CMSCFT was set to be zero: $J(\boldsymbol{r}) = 0$. Fig. 1 shows the density profiles of conventional SCFT. Just as expected, little difference between density profile of the two models was noticed even when incompressibility is only about $\zeta = 10$. Furthermore, from Fig. 2 we can observe a clear linear dependence that shows precisely how CMSCFT asymptotically converges to conventional SCFT in the limit $\zeta \to \infty$:

$$\|\bar{\rho}_0 - 1\|_\infty = C \cdot \frac{1}{\zeta},$$

where $\bar{\rho}_0 = \rho_A + \rho_B$ is the total density of both segments.

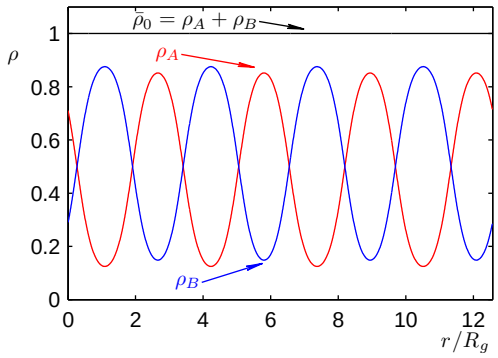

FIG. 1: Density profiles for lamellae phase without hard wall confinement. ρ_A denotes density of A-segments, ρ_B for B-segments, and $\bar{\rho}_0$ for total density of all segments.

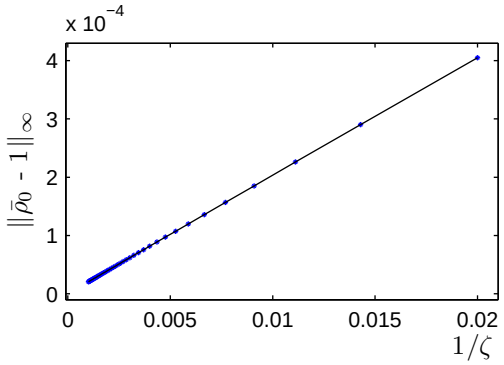

FIG. 2: Total density $\bar{\rho}_0$ of CMSCFT converges to 1 when ζ tends to ∞.

Confinement Effects and Boundary Layer

Confinement effects, such as density depletion, surface oscillation, and surface segregation, have generated increasing interests in the community. Although plenty of efforts have been made, there is still lots of work to do. As stated in section I., the conventionally used MSCFT skill developed by Matsen [23] is not so satisfactory. Moreover, no method has been proposed to calculate boundary layer thickness in numerical simulations. In this section, we are going to show that CMSCFT gives a satisfactory simulation of all confinement effects. Furthermore, boundary layer thickness calculated in CMSCFT can agree well with real physical system, as long as boundary potential is well constructed.

Surface Depletion

Equilibrium surface force measurement of two liquid PB sample by Israelachvili *et al.* [13] shows no oscillation but steeply repulsive force approaching the boundaries. For this kind of system, modified Lennard-Jones potential is appropriate to characterize the hard wall influence:

$$J(\boldsymbol{r}) = \begin{cases} 4\alpha \left[\left(\frac{\sigma}{d(\boldsymbol{r})} \right)^{12} - \left(\frac{\sigma}{d(\boldsymbol{r})} \right)^{6} \right] + \alpha & d(\boldsymbol{r}) \leqslant \sqrt[6]{2}\sigma \\ 0 & \text{otherwise,} \end{cases} \tag{20}$$

where $d(\boldsymbol{r})$ is the distance of the point $\boldsymbol{r}$ to boundary. Note that polymer-boundary interaction only happens when segments are adjacent to the boundary. And $b = \sqrt{6/N}R_g$ is statistical segment length in Gaussian chain model of block copolymer. Consequently, we can fix $\sigma = b/2$ in Eq. (20), e.g., $\sigma \sim 0.1R_g$ when $N = 120$ and $b \approx 0.22R_g$. Finally, α in (20) is fixed to control the magnitude of Lennard-Jones potential. Surface interaction energy is $\sim k_BT$ according to Israelachvili's measurement [12, 13]. Hence we simply set $\alpha = 1$ here. Specifically, the following Lennard-Jones potential is used in our calculation for convenience:

$$J(\boldsymbol{r}) = \begin{cases} 4 \cdot \left[\left(\frac{0.1}{d(\boldsymbol{r})} \right)^{12} - \left(\frac{0.1}{d(\boldsymbol{r})} \right)^{6} \right] + 1 & d(\boldsymbol{r}) \leqslant 0.1 \times \sqrt[6]{2} \\ 0 & \text{otherwise.} \end{cases} \tag{21}$$

Fig. 3 shows density profiles of the confined system. By comparing with Fig. 1, we note that, hard wall confinement does not change the pattern of density profile in the bulk. Fig. 4 illustrates the profile of boundary layer. The red dots are the simulations of CMSCFT, the blue line is the emprical formula (1), and the dotted line is Q. Wang's exponential profile for the "best" numerical behavior. Note that all three profiles share the same boundary layer thickness δ in this manner:

$$\delta = \int_{\tilde{r}}^{r_0} (\psi - \rho(r))\, dr, \tag{22}$$

where ψ, a constant, is total density in the bulk where far enough away from boundaries, $\tilde{r}$, shown in Fig. 4, is the position where total density $\bar{\rho}_0$ starts to increase, and r_0 is a distance far away from boundaries where polymer density reach bulk density: $\rho(r_0) = \psi$. Boundary layer thickness, according to formula (22), is $\sim 0.04R_g$ and $0.014R_g$ respectively. From Fig. 4, we note that CMSCFT simulation perfectly match the emprical Hyperbolic tangent profile (1).

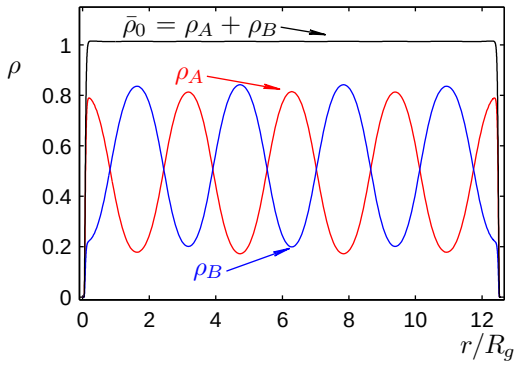

FIG. 3: Density profiles for lamellae phase with hard wall confinement, where Lennard-Jones potential (21) is used and ζ is set to be 10. Notations are used the same as Fig. 1.

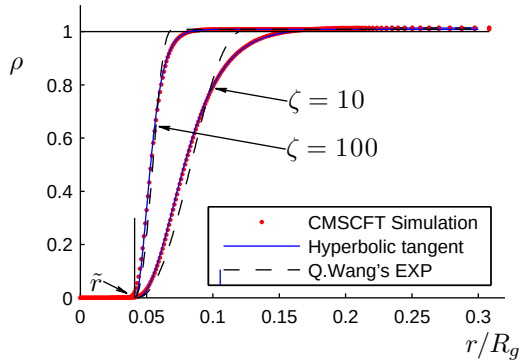

FIG. 4: Boundary layer profile near hard surface. Again, Lennard-Jones potential (21) is used and ζ is set to be 10, 100 respectively. Comparison with emprical Hyperbolic tangent (1) and Q. Wang's EXP in MSCFT [27] is given with the same layer thickness.

Boundary Layer Thickness

Boundary layer thickness is also very important in various applications. However, current simulation method, such as Monte-Carlo and MSCFT, needs to determine layer thickness beforehand. On the contrary, CMSCFT can automatically determine the layer thickness with given boundary potential. We have investigated the relationships between layer thickness and various parameters in CMSCFT. Again, Lennard-Jones potential (20) is used in this section, and formula (22) is served as the definition of layer thickness. We didn't see notable influence of parameters: χN, f, and L. However, a simple dependence of δ on ζ (with all

other parameters fixed) is observed, as shown in Fig. 5:

$$\delta \approx 0.123\frac{1}{\sqrt{\zeta}} + 0.008, \tag{23}$$

where specified Lennard-Jones (21) is used, and $\tilde{\boldsymbol{r}}$ in (22) is fixed so that $\bar{\rho}_0(\tilde{\boldsymbol{r}}) = 10^{-4}$. We note that the zeroth-order constant in the above formula is much smaller than the first-order coefficient. So, it is reasonable to say that the above relationship should be exactly direct proportion:

$$\delta = C\frac{1}{\sqrt{\zeta}} \tag{24}$$

As shown in Fig. 6, σ in Lennard-Jones potential (20) hardly influence the shape of Boundary Layer profile but will affect the position $\tilde{r}$ where total density $\bar{\rho}_0$ starts to increase. Furthermore, $\tilde{r}$ relies almost linearly on σ. Note that here $\zeta = 10$.

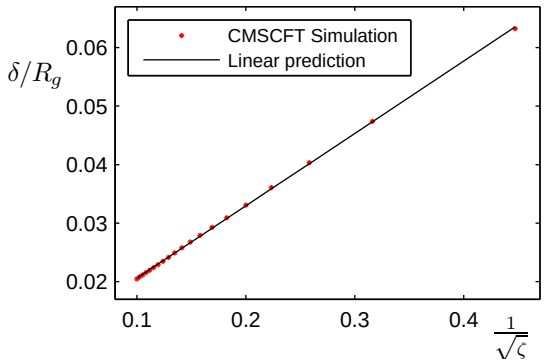

FIG. 5: Layer thickness $\delta - \zeta$ dependence. Comparison between CMSCFT simulation and linear prediction (23) is given.

Surfaces Oscillations

It's suggested by experimental measurements [18] that, surfaces force can be oscillatory to some extent. Hence, it is necessary to consider oscillatory boundary potentials. In this section, we add the following oscillatory behavior to Lennard-Jones potential for convenience:

$$J(\boldsymbol{r}) = \begin{cases} \left\{4\alpha\left[\left(\frac{\sigma}{d(\boldsymbol{r})}\right)^{12} - \left(\frac{\sigma}{d(\boldsymbol{r})}\right)^{6}\right] + \alpha\right\} \cdot \left\{\cos[2n\pi \cdot \frac{d(\boldsymbol{r})}{\sigma}] + 1\right\} & d(\boldsymbol{r}) \leqslant \sqrt[6]{2}\sigma \\ 0 & \text{otherwise.} \end{cases} \tag{25}$$

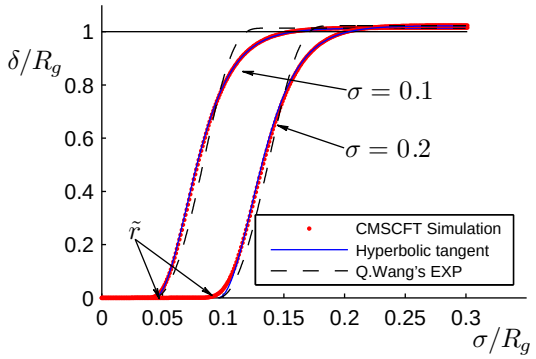

FIG. 6: Boundary Layer $-\sigma$ dependence. ζ is set to be 10. Comparison with emprical Hyperbolic tangent (1) and Q. Wang's EXP in MSCFT [27], in the condition of a same layer thickness, is given.

Fig. 7 shows the profile of oscillatory potential (25) with $n = 12$, $\sigma = 0.1$, and $\alpha = 1$. We note that, when $d(\boldsymbol{r}) \geqslant 0.075R_g$ the potential profile shown in this figure looks pretty close to the surface force profile measured by Israelachvili *et al.* [18]. Oscillation in the corresponding boundary layer profile of total density is too weak to be observe directly. Thus we have to compare this profile with non-oscillating profile which corresponds to Lennard-Jones potential (21). From Fig. 8, which shows the difference between these two boundary layer profiles, we can see an obvious oscillation in the range $d(\boldsymbol{r}) \in [0.035R_g, 0.08R_g]$ where the total density is increasing.

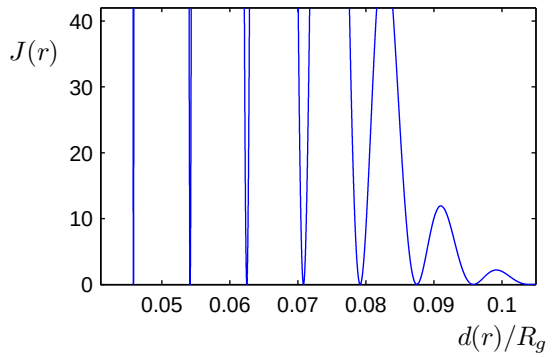

FIG. 7: Oscillatory Boundary Potential (25) with $n = 12$, $\sigma = 0.1$, and $\alpha = 1$.

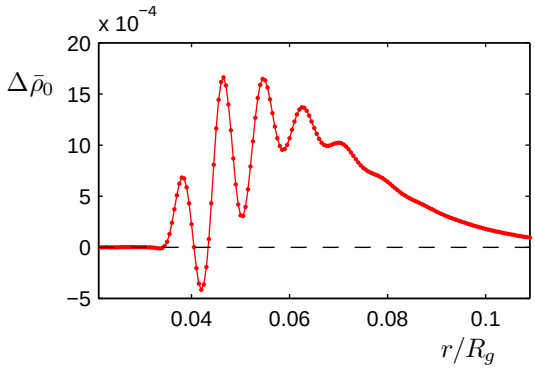

FIG. 8: The difference between Oscillatory Boundary Layer with oscillatory potential shown in Fig. 7 and Non-oscillating Boundary Layer with Lennard-Jones potential (21). Note that here ζ is set to be 20.

Entropy-Driven Surface Segregation

In 1992, Mohan Sikka *et al.* carried out an experiment about Entropy-driven surface segregation in block copolymer melts [14]. They showed that conformationally smaller block would preferentially segregate to both the solid and air interface, which have little relationship with surface energy. In addition, they attributed this surface segregation to configurational entropy loss and conformational asymmetry of block polymer.

In our simulation, although boundary potential of both segments are set to be equal (the same as specified Lennard-Jones (21)), i.e.,

$$J_A(\boldsymbol{r}) = J_B(\boldsymbol{r}) = J(\boldsymbol{r})$$

we still observe surface segregation just as concluded by Mohan [14]. According to segment density distribution formula (14), we can easily define the reduced distribution function of the (sN)th segment on a copolymer chain (where Q is defined by formula (14)):

$$\rho(\boldsymbol{r}, s) = \frac{V \cdot q(\boldsymbol{r}, s) \cdot q^+(\boldsymbol{r}, 1-s)}{Q} \tag{26}$$

Fig. 9 shows how all segments along a copolymer chain distribute at some distance off the boundary, where the separation of A- and B-segments occurs at $f = 0.48$. It is obvious from this figure that segment segregation exists only at the vicinity of boundary, and decreases rapidly into the bulk. Both ends are much denser than other segments near boundary. In addition, A-end are even more denser than B-end as concluded by Mohan [14], although

there is only little asymmetry in the copolymers ($f = 0.48$). In Fig. 9, we observe another interesting phenomenon. It seems that surface segregation only relates to segments near the ends. Segments away from the ends have a similar distribution profile that has little dependence on position $\boldsymbol{r}$ in the vicinity of boundaries.

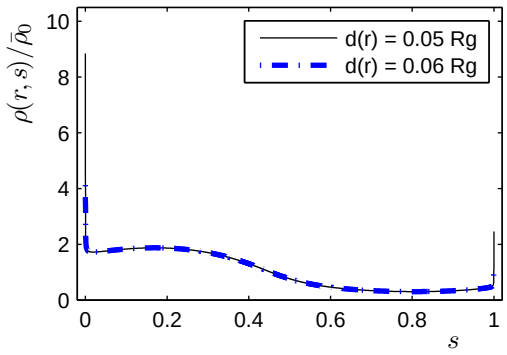

FIG. 9: Reduced distribution of segments along a whole chain at two different distance off the boundary $d(\boldsymbol{r}) = 0.05R_g$ and $0.06R_g$ respectively.

Fig. 10 shows how certain segment (A-end, segment near A-end, and A-B joins) distributes over space. It can be seen that, the end of the segments is likely to assemble at hard surface. However this effect decreases quickly into the bulk. Fig. 10 shows more clearly that surface segregation is only related to segments near the ends. Even when $s = 0.0025$, which is prety near A-end, we only observe very weak accumulation near surface. Moreover, solid wall does not have noticable influence of the reduced distribution of A-B joins ($f = 0.48$).

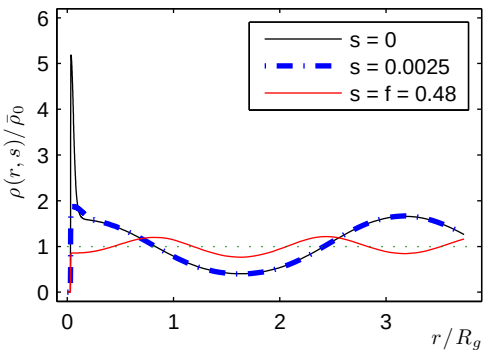

FIG. 10: Reduced distribution of some segments on copolymer chain. A-ends ($s = 0$), some A-segments near A-end ($s = 0.0025$), and A-B joins ($s = f = 0.48$) respectively.

CONCLUSION

We propose a modified Compressible Model based SCFT (CMSCFT) for confined diblock copolymer melt system. Unlike the conventionally used MSCFT developed by Matsen [23], which constraints the total density to be a predesigned profile ϕ_0, CMSCFT makes no artificial constraints: The boundary potential is fixed by experimental inspiration and physical analysis, and model compressibility $1/\zeta$ can be fixed by comparison between simulation results (24) and experimental measurements. So, with properly reconstructed boundary potential and carefully chosen compressibility parameter $1/\zeta$, the CMSCFT can be used to simulate a real physical system.

Furthermore, CMSCFT gives a successful simulation of all known hard surface effects: surface density oscillations [11, 13], surface depletion [9, 10], and surface segregation [14]. First of all, boundary layer profile of CMSCFT simulations match perfectly with the emprical Hyperbolic-tangent profile. However the "best" profile propose by Q. Wang *et al.* has a notable difference with CMSCFT simulations. Secondly, CMSCFT method can conveniently calculate boundary layer thickness, and give the dependences between layer thickness and some model parameters. Then we show that surface oscillation is attributed to oscillatory boundary potential in CMSCFT. Finally, CMSCFT can well reproduce the surface segregation effect: chain ends enriches near hard surface and chain ends of shorter blocks are much denser than those of the longer ones. Consequently, we claim that CMSCFT can be a promising tool in confined copolymer system simulations. A final remark: although we only derive the model under diblock copolymer system, the extention to more complicated architecture copolymer (like triblock and star copolymer) should be straightforward.

ACKNOWLEDGMENTS

The authors thank Prof. An-Chang Shi for helpful suggestion on the selection of segments interaction parameters ($\varepsilon_{AA}, \varepsilon_{BB}, \varepsilon_{AB}$). Helpful discussions with colleagues: Xiuyuan Cheng, Kai Jiang, and Han Wang are also very thankful. PWZ would like to thank the financial support by the special funds for Major State Research Projects (2005CB321704), and National Natural Science Foundation of China (50930003).

* pzhang@pku.edu.cn

[1] Park, C.; Yoon, J.; Thomas, E.L. **Polymer** 2003, 44, 6725-6760.

[2] L. Leibler **Macromolecules** 13 1602 (1980)

[3] A. N. Semenov **Sov. Phys. JETP** 61 733 (1985)

[4] M. W. Matsen, M. Schick **Phys. Rev. Lett.** 74 4225 (1995)

[5] ANC SHI *Developments in Block Copolymer Science and Technology* , 2004, 265-293.

[6] Weihua Li, Robert A. Wickham, and Robert A. Garbary. **Macromolecules** 2006, 39, 806-811

[7] G. J. A. Sevink, A. V. Zvelindovsky, B. A. C. van Vlimmeren, N. M. Maurits, and J. G. E. M. Fraaije. **J. Chem. Phys.** 110, 2250 (1999)

[8] S. Asakura and F. Oosawa. **J. Chem. Phys.** 22, 1255 (1954)

[9] C. Allain, D. Ausserre, F. Rondelez. **Phys. Rev. Lett.** 49, 1694 (1982)

[10] J. N. Israelachvili, S. J. Kott, **J. Chem. Phys.** 88, 7162 (1988)
R. G. Horn, J. N. Israelachvili. **Macromolecules** 21, 2836 (1988)

[11] H. K. Christenson, D. W. R. Gruen, R. G. Horn, and J. N. Israelachvili. **J. Chem. Phys.** 87, 1834 (1987)

[12] J. N. Israelachvili, and G. E. Adams. **J. Chem. Soc. Faraday Trans1 74** 975 (1978)

[13] J. N. Israelachvili and Stephen J. Kott. **J. Chem. Phys.** 88, 7162 (1988)

[14] M. Sikka, N. Singh, A. Karim, F. S. Bates. **Phys. Rev. Lett.** 70, 307 (1993)

[15] P.G. de Gennes. **Adv. Colloid Interface Sci.** 1987, 27, 189.
S. Wu. *PolymerInterfaces and Adhesion* , 1982 (Dekker, New York).

[16] J. F. Joanny, L. Leibler, and P. G. de Gennes. **J. Polym. Sci., Polym. Phys.** 17 1073 (1979)

[17] J. D. van der Waals, **Z. Phys. Chem.** 13 657 (1894)

[18] R. G. Horn, J. N. Israelachvili. **Macromolecules** 1988, 21, 2836-2841

[19] Dzina Kleshchanok, Remco Tuinier and Peter R Lang. **J.Phys.:Condens. Matter** 20 073101 (2008)

[20] Derjaguin B V. **Kolloid Z.** 69 155 (1934)

[21] Israelachvili J N. *Intermolecular and Surface Forces* 2nd edn (London: Academic)

[22] M. Kikuchi, K. Binder **J. Chem. Phys.** 101 3367 (1994); **Europhys. Lett.** 21 427 (1997)

[23] M. W. Matsen **J. Chem. Phys.** 106 7781 (1997)

[24] T. Geisinger, M. Müller, K. Binder **J. Chem. Phys.** 111 5241 (1999)

[25] H. Y. Chen, G. H. Fredrickson **J. Chem. Phys.** 116 1137 (2002)

[26] W. H. Li, R. A. Wickham, R. A. Garbary **Macromolecules** 39 806 (2006)

[27] Dong Meng, Qiang Wang **J. Chem. Phys.** 126 234902 (2007)

[28] Eugene Helfand **J. Chem. Phys.** 62 999 (1975)

[29] Glenn H. Fredrickson *The Equilibrium Theory of Inhomogeneous Polymers* (Oxford University Press, OXFORD, 2006)